Detrimental Effects of IFN-γ on an Epidermolysis Bullosa Simplex Cell Model and Protection by a Humanized Anti–IFN-γ Monoclonal Antibody

Cedric Badowski[1], Tong San Tan[1,2], Teimur Aliev[3], David Trudil[4], Maria Larina[5], Victoria Argentova[6], Muhammad Jasrie Firdaus[1,2,7], Paula Benny[1], Vivien S.T. Woo[1,8] and E. Birgitte Lane[1,2,8]

Epidermolysis bullosa is a group of severe skin blistering disorders, which currently have no cure. The pathology of epidermolysis bullosa is recognized as having an inflammatory component, but the role of inflammation in different epidermolysis bullosa disorders is unclear. Epidermolysis bullosa simplex (EBS) is primarily caused by sequence variants in keratin genes; its most severe form, EBS generalized severe, is characterized by aggregates of keratin proteins, and cell models of EBS generalized severe show constitutively elevated stress. IFN-γ is a major mediator of inflammation, and we show that the addition of IFN-γ alone to disease model keratinocytes promotes keratin aggregation, decreases cell–cell junctions, delays wound closure, and reduces cell proliferation. IFN-γ exposure weakens the intercellular cohesion of monolayers on mechanical stress, with IFN-γ–treated EBS monolayers more fragmented than IFN-γ–treated wild-type monolayers. A humanized monoclonal antibody to IFN-γ neutralized the detrimental effects on keratinocytes, restoring cell proliferation, increasing cell–cell adhesion, accelerating wound closure in the presence of IFN-γ, and reducing IFN-γ–mediated keratin aggregation in EBS cells. These suggest that treatment with IFN-γ blocking antibodies may constitute a promising new therapeutic strategy for patients with EBS and may also have ameliorating effects on other inflammatory skin diseases.

JID Innovations (2022);**2:**100096 doi:10.1016/j.xjidi.2022.100096

INTRODUCTION

Epidermolysis bullosa simplex (EBS) is an inherited skin fragility disorder caused by detrimental sequence variants of keratin genes *KRT5* or *KRT14* (Bonifas et al., 1991; Coulombe et al., 1991; Lane et al., 1992; reviewed in Porter and Lane, 2003). Mutation at the helix boundary motifs of the keratin protein rod domain (e.g., keratin 14 [K14] R125C) results in severe phenotypes such as EBS Dowling-Meara (now classified as EBS generalized severe), in which aggregates of mutant keratin proteins have been observed in vivo (Ishida-Yamamoto et al., 1991) and in cultured cells (Coulombe et al., 1991). These aggregates are characteristic of severe EBS (Anton-Lamprecht and Schnyder, 1982) and are less prominent in milder forms of EBS, suggesting that the presence of aggregates is associated with the severity of the disease (Coulombe et al., 1991; reviewed in Lane, 1994; Letai et al., 1993). Thus, reducing these keratin aggregates may be a useful target step in developing an EBS therapy (Werner et al., 2004).

Aside from the keratin defects that trigger the disease, EBS and other forms of EB are known to be associated with inflammation. Inflammation is a complex immunological reaction triggered by tissue injury, infection, and a range of other stresses. It involves several different immune cell types that migrate, proliferate, and produce cytokines, ILs, and IFNs in an orchestrated manner (reviewed by Schroder et al., 2004). Studies have shown that serum samples from patients with dystrophic EB (a skin fragility disorder caused by sequence variants in *COL7A1* encoding collagen 7) contain high levels of inflammatory molecules such as IL-1β, IL-2, IL-6, IL-12, and IFN-γ (Annicchiarico et al., 2015; Kawakami et al., 2005). Patients with EBS also display higher systemic levels of inflammatory mediators such as IFN-γ, a cytokine (type II IFN family) primarily secreted by NK cells, and activated T lymphocytes (reviewed by Castro et al., 2018), although not as much as patients with dystrophic EB (Annicchiarico et al., 2015).

[1]*Institute of Medical Biology, Agency for Science, Technology and Research (A*STAR), Singapore, Singapore;* [2]*Skin Research Institute of Singapore (SRIS), Agency for Science, Technology and Research (A*STAR), Singapore, Singapore;* [3]*Faculty of Chemistry, Lomonosov Moscow State University, Moscow, Russia;* [4]*NHDetect Corporation, Reisterstown, Maryland, USA;* [5]*Shemyakin–Ovchinnikov Institute of Bioorganic Chemistry, Russian Academy of Sciences, Moscow, Russia;* [6]*Faculty of Biology, Lomonosov Moscow State University, Moscow, Russia;* [7]*Lee Kong Chian School of Medicine, Nanyang Technological University, Singapore, Singapore; and* [8]*Department of Pathology, Yong Loo Lin School of Medicine, National University of Singapore, Singapore, Singapore*

*Correspondence: E. Birgitte Lane, Skin Research Institute of Singapore (SRIS), Agency for Science, Technology and Research (A*STAR), Immunos Building, 8A Biomedical Grove, Singapore 138648, Singapore. E-mail: birgit.lane@sris.a-star.edu.sg*

Abbreviations: EB, epidermolysis bullosa; EBS, epidermolysis bullosa simplex; K14, keratin 14; KC, keratinocyte; KSFM, keratinocyte serum-free medium; STAT, signal transducer and activator of transcription; WT, wild type

Received 10 February 2021; revised 14 October 2021; accepted 17 November 2021; accepted manuscript published online XXX; corrected proof published online XXX

Cite this article as: JID Innovations 2022;2:100096

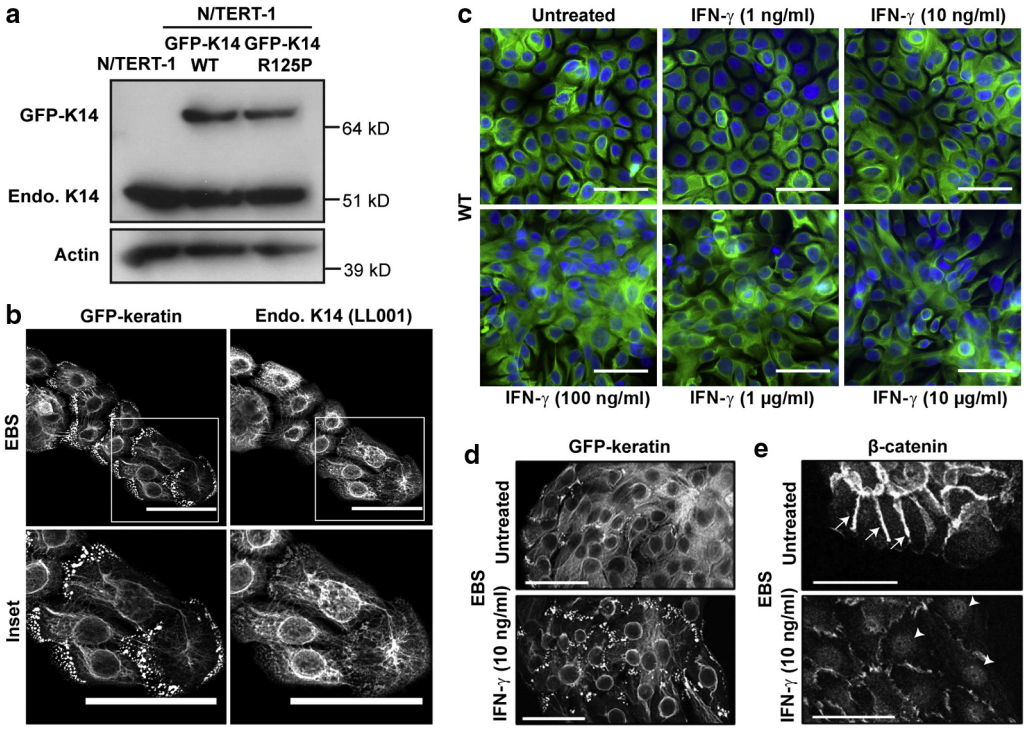

Figure 1. Characteristics of transfected model cell lines. (**a**) Expression levels of the transfected keratins GFP-K14 WT (normal) and GFP-K14 R125P (EBS mutant) are similar in the two lines. GFP-tagged and endogenous (Endo.) K14 seen in cell lysates of subconfluent N/TERT-1 KCs stably expressing GFP-tagged K14 WT or GFP-tagged K14 R125P. Actin as loading control (a similar but nonidentical immunoblot is shown in Tan et al. [2021] wherein these lines are described.) (**b**) Fluorescence images of EBS KCs comparing GFP (transfected) fluorescence (left) with antibody staining (LL001) (right). EBS (GFP-K14 R125P) keratin generates aggregates but also contributes to filaments of Endo. K14. (**c**) IFN-γ treatment does not affect keratin filaments in WT KCs (subconfluent WT KCs +/− IFN-γ [concentrations indicated] for 7 days). (**d, e**) EBS KCs ± IFN-γ (10 ng/ml) for 7 days show immunostaining of β-catenin. Arrows and arrowheads indicate membrane and nuclear localization of β-catenin, respectively. Bar = 50 μm. EBS, epidermolysis bullosa simplex; Endo., endogenous; K14, keratin 14; WT, wild type.

In this study, we show how inflammation may directly exacerbate the EBS phenotype through the effect of IFN-γ. We show that IFN-γ promotes formation of EBS generalized severe mutant keratin protein aggregates and that IFN-γ exposure reduces cell—cell adhesion, slows cell proliferation, increases nondirectional cell migration, and delays wound closure. IFN-γ also compromises intercellular strength of EBS keratinocyte (KC) monolayers and increases fragility of EBS organotypic cultures on mechanical agitation. Finally, we show that these detrimental biological effects of IFN-γ can be overcome if the action of IFN-γ is neutralized by a humanized mAb to human IFN-γ. Humanized antibodies therefore represent potentially valuable therapeutic agents that could be directly administered in patients with EBS and may promote the healing of existing blisters and reduce the occurrence of new ones.

RESULTS AND DISCUSSION

IFN-γ promotes the aggregation of mutant keratin proteins in EBS KCs

In view of the known link between EBS and skin inflammation, we investigated whether inflammation could affect the severity of the EBS phenotype. If so, then disrupting the signaling pathway of IFN-γ, a major mediator of inflammation, might have therapeutic value. We used a human EBS disease model KC cell line, N/TERT-1 GFP-K14 R125P cells, which stably expresses a GFP-tagged mutant K14 R125P (referred to as EBS KC in this study), and compared the cell line with a similarly generated cell line expressing GFP-tagged wild-type (WT) K14 (i.e., N/TERT-1 GFP-K14 WT cells, referred to as WT KCs in this study). Figure 1 highlights some baseline characteristics of these transfected cells in the context of the study. The EBS KCs express keratin aggregates in tissue culture, a classic hallmark of severe EBS (Figure 2a), but after reaching confluence, they progressively lose aggregates as they become quiescent (Common et al., manuscript in preparation). Using this tissue culture disease model, we asked whether IFN-γ itself could have an effect on any of the phenotypic characteristics that define EBS. Using a semiautomated image analysis algorithm (Tan et al., 2021), we assessed keratin aggregate formation in the presence and absence of human recombinant IFN-γ added to the culture medium. When subconfluent EBS KCs were treated with IFN-γ, the cells retained abundant keratin aggregates for at least 7 days (Figure 2a and b), that is, well beyond confluence. This effect of IFN-γ on keratin aggregation was significant at concentrations from 10 ng/ml to 10 μg/ml compared with that observed in untreated control (Figure 2b). IFN-γ treatment did not alter the keratin filament networks in WT KCs (Figure 1c). From these experiments, we selected 10 ng/ml and 100 ng/ml IFN-γ (which give significant amounts of keratin aggregation) for subsequent experiments. Postconfluent EBS KCs (from which keratin

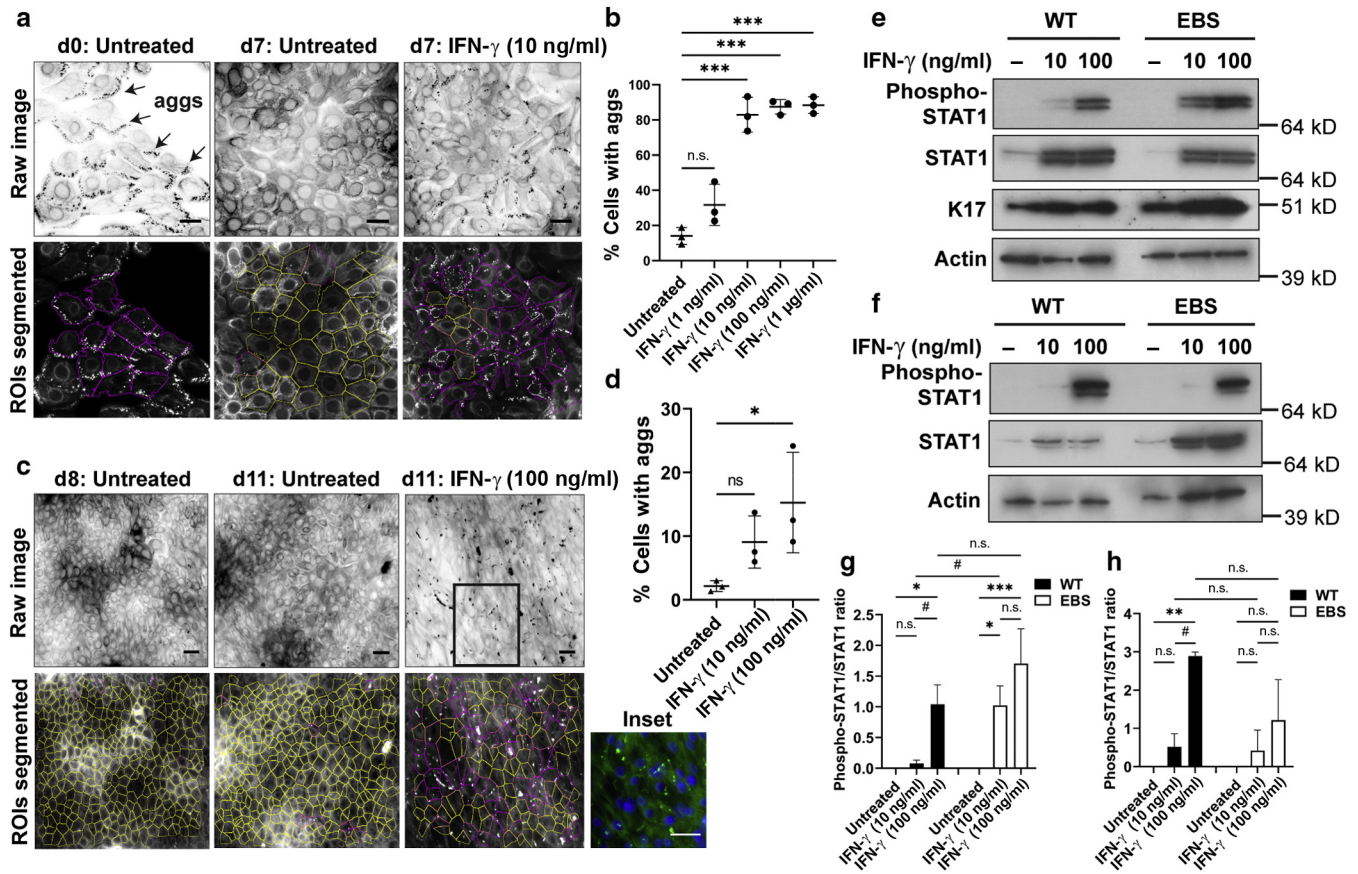

Figure 2. IFN-γ promotes aggregation of mutant keratin proteins in EBS KCs. (**a, b**) Subconfluent EBS KCs (before treatment) ± IFN-γ (10 ng/ml) for 7 days (inverse grayscale). Bar = 20 μm. (**c, d**) Two-day postconfluent EBS KCs ± IFN-γ (10 ng/ml) for 3 days (inverse grayscale). Bar = 40 μm. Images segmented using ImageJ algorithm scoring ROIs with (red) or without (yellow) aggs. (**b, d**) At least 300 cells per group counted in (**a**) and 1,800 cells per group in (**c**). Mean ± SD for n = 3 per group. $^{*}P < 0.05$ and $^{***}P < 0.001$ versus untreated group (ANOVA). (**e, f**) Immunoblotting shows phospho-Tyr701 STAT1, total STAT1, and K17 proteins in subconfluent WT and EBS cell lysates ± IFN-γ (concentrations indicated) for 5 days in (**e**) and in 2-day postconfluent WT and EBS cell lysates ± IFN-γ (concentrations indicated) for 3 days in (**f**). Actin as loading control. (**g, h**) Ratios of densitometry values (phospho-STAT1/STAT1) obtained using ImageJ. Mean ± SD, (**g**) n = 3 per group for (**e**), (**h**) n = 2 per group for (**f**). $^{*}P < 0.05$, $^{**}P < 0.01$, and $^{***}P < 0.001$ versus untreated group; $^{\#}P < 0.05$ versus WT IFN-γ (10 ng/ml) group (ANOVA). agg, aggregate; d, day; EBS, epidermolysis bullosa simplex; K17, keratin 17; n.s., nonsignificant; ROI, region-of-interest; STAT, signal transducer and activator of transcription; WT, wild type.

aggregates had disappeared) were next exposed to IFN-γ for 3 days (Figure 2c), where we observed a reappearance of keratin aggregates with increasing IFN-γ concentrations. This indicates a causative, although probably indirect, relationship between IFN-γ exposure and keratin aggregates in EBS KCs (Figure 2d). Induction of keratin aggregates by IFN-γ suggests that IFN-γ is likely to exacerbate the disease phenotype of EBS.

IFN-γ induces changes indicative of KC activation associated with stress

On treating KCs with IFN-γ (10 ng/ml) for 5 days, immunoblot analysis showed an increase in phospho-Tyr701 signal transducer and activator of transcription (STAT) 1, which lies downstream in the IFN-γ inflammatory signaling pathway (Platanias, 2005), in both WT and EBS KCs. IFN-γ–treated EBS KCs showed a much higher level of phospho-Tyr701 STAT1 than IFN-γ–treated WT KCs, suggesting that EBS KCs are stress primed or susceptible to intrinsic inflammation (Figure 2e and g). Keratin 17 is a stress response keratin known to be induced by IFN-γ (Bonnekoh et al., 1995), and as expected, this was also observed to be elevated by IFN-γ in both WT and EBS KCs (Figure 2e). However, in postconfluent cells treated with IFN-γ, phospho-Tyr701 STAT1 levels were not significantly different between WT and EBS KCs (Figure 2f and h), possibly owing to fewer aggregates in this postconfluent IFN-γ–treated mutant cells.

We investigated the mechanisms underlying the increased mutant keratin aggregation induced by IFN-γ treatment. IFN-γ–treated EBS KCs were less densely packed, with increased intercellular spaces in the cell sheet. In contrast, untreated EBS KCs were able to grow to full confluence and remained relatively compact, with few to no intercellular spaces and very few keratin aggregates (Figure 3a). IFN-γ treatment of EBS KCs led to changes in cell shape, with cells becoming less compact and more spread (Figure 3a–c). This was accompanied by changes in β-catenin distribution, with a reduction in membrane localization and some nuclear localization (Figures 3b and 1d and e), suggesting reduced cell junctions and thus possibly weaker cell–cell adhesion. Desmoplakin immunostaining also appeared less focused at the cell periphery in IFN-γ–treated EBS KCs (Figure 3c).

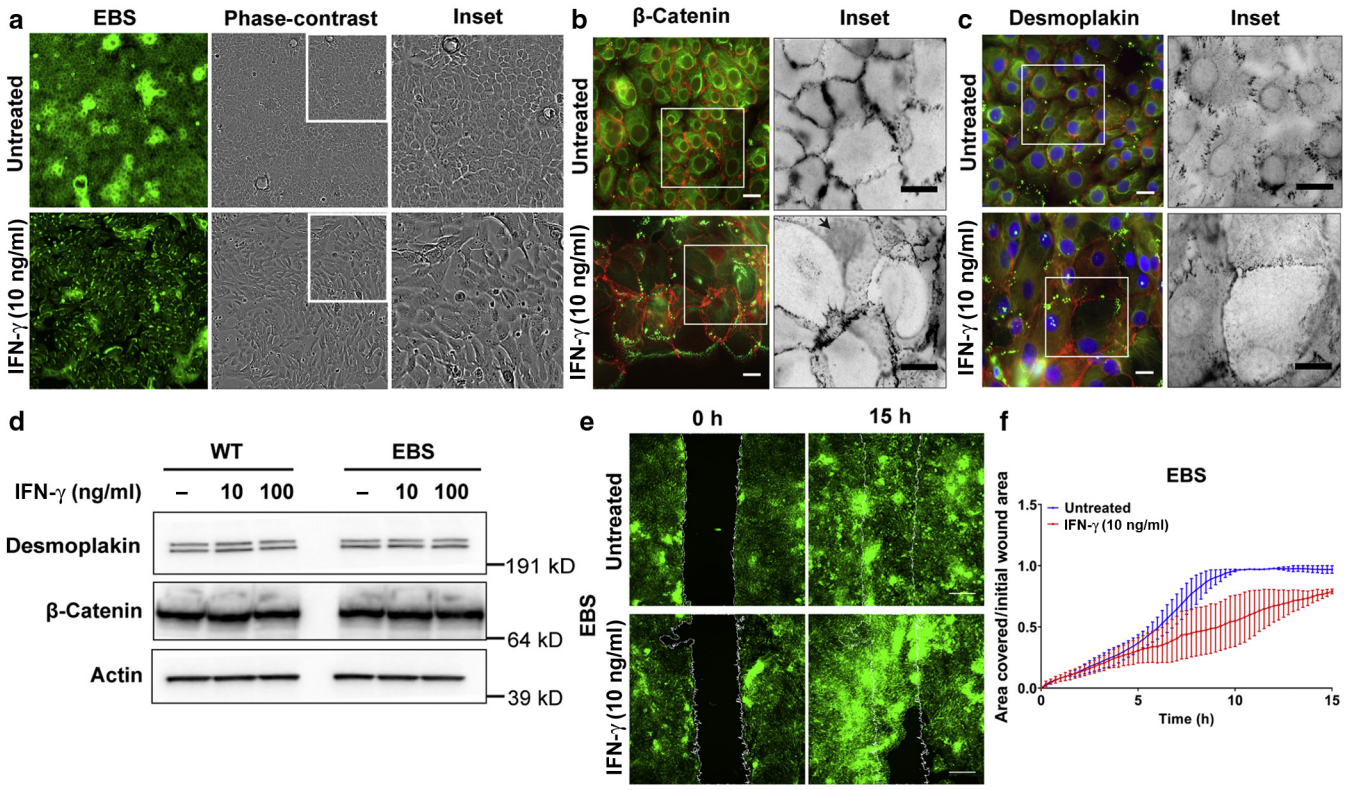

Figure 3. IFN-γ treatment reduces cell–cell adhesions in EBS KCs and leads to nondirectional migration. (**a**) Fluorescence and phase-contrast images of EBS KCs ± IFN-γ (10 ng/ml) for 4 days. (**b, c**) EBS KCs ± IFN-γ (10 ng/ml) for 7 days show immunostaining of (**b**) β-catenin (some nuclear localization is indicated by black arrow) and (**c**) desmoplakin I/II. Inset shows inverse grayscale of ROIs. Bar = 20 μm. (**d**) Immunoblotting desmoplakin I/II and β-catenin proteins in subconfluent WT and EBS cell lysates ± IFN-γ (concentrations indicated) for 5 days. Actin as loading control. (**e, f**) Sequential images and graphs of EBS KCs closing a wound gap, ± IFN-γ (10 ng/ml) added 48 h before closure was initiated on removal of the silicone culture insert. 0 h shows initial wound gap, whereas 5–15 h show remaining wound gap. Bar = 200 μm. Mean ± SD, n = 2 different fields within same wound gap. EBS, epidermolysis bullosa simplex; h, hour; ROI, region-of-interest; WT, wild type.

However, immunoblotting analyses revealed that both desmoplakin I/II and β-catenin protein expression levels were similar with or without IFN-γ treatment (Figure 3d), suggesting that IFN-γ decreases cell–cell adhesion by causing redistribution of junction components within the cell (Figure 3b and c), rather than by degrading proteins or reducing their synthesis. These observed changes are in keeping with a generalized stress-induced or wound-induced activation of the KCs (reviewed by Freedberg et al., 2001; Kirfel and Herzog, 2004; Singer and Clark, 1999).

Persistent inflammation is associated with ineffective wound healing (reviewed by Eming et al., 2007), and therefore, wound-healing-analogous gap closure behavior was investigated in this culture model. Using 2-chambered ibidi silicone inserts with a removable central wall of consistent width (ibidi, Gräfelfing, Germany), gap closure experiments were carried out in the presence and absence of IFN-γ. With IFN-γ, EBS KCs displayed slower and less effective gap closure rates than EBS controls without IFN-γ (Figures 3e and f). IFN-γ–treated cells also consistently showed irregular lateral and forward motion at the wound edges, with gaps in the epithelial sheet appearing behind the advancing edge as the cells stretched, plus some highly motile scattered cells breaking away from the edges and moving randomly on their own; this was indicative of a loss of directional cell migration (Supplementary Movies S1 and S2) and less coherent movement in wound healing.

IFN-γ weakens intercellular cohesion of EBS KCs

From these results, it appears that under inflammatory conditions induced by IFN-γ, both EBS and WT KCs are likely to be less adherent to each other than untreated KCs. If this holds true in vivo, it will have significant consequences for the mechanical resilience of the epidermis. Monolayers of IFN-γ–treated EBS and WT KCs were therefore tested, specifically for their ability to maintain a coherent epithelial sheet structure when subjected to mechanical stress, applied as repeated rotational inversion. Both WT and EBS IFN-γ–treated monolayers were more easily fragmented by this mechanical stress than untreated ones, with the IFN-γ–treated EBS monolayers being even more fragmented than IFN-γ–treated WT monolayers ($^{\#\#\#}P < 0.001$) (Figure 4a–c). This confirms that the inflammatory state induced by IFN-γ exacerbates EBS KC sheet fragility in vitro ($^{***}P < 0.001$) (Figure 4c). Some loss of cohesion is also seen in the WT cells, but the difference is less dramatic ($^{**}P < 0.01$) (Figure 4c). Preliminary experiments using three-dimensional organotypic cultures also showed that on mechanical agitation, IFN-γ–treated EBS organotypics showed evidence of tissue breakdown in the lower cell layers of the stratified epithelium, which was not seen in IFN-γ–treated WT

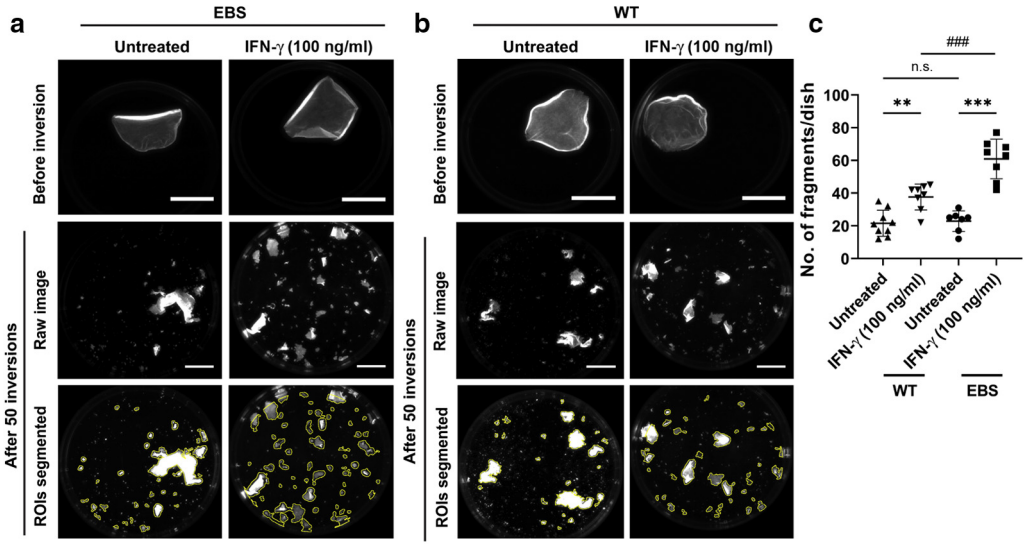

Figure 4. IFN-γ weakens intercellular adhesion strength of KC monolayer. (**a, b**) Fragmentation of WT and EBS KC monolayers released by dispase treatment (see Materials and Methods) after 50 rounds of rotational inversions. Yellow-outlined ROIs denote cell sheet fragments of at least 500 pixels area. Bar = 10 mm. (**c**) Quantitative data from WT and EBS monolayer ± IFN-γ (100 ng/ml) for 3 days after confluence, presented as average number of fragments. Mean ± SD, n = 7–9 per group. $^{\#\#\#}P < 0.001$ versus IFN-γ–treated WT group; $^{**}P < 0.01$ and $^{***}P < 0.001$ versus untreated group (ANOVA). EBS, epidermolysis bullosa simplex; No., number; n.s., nonsignificant; ROI, region-of-interest; WT, wild type.

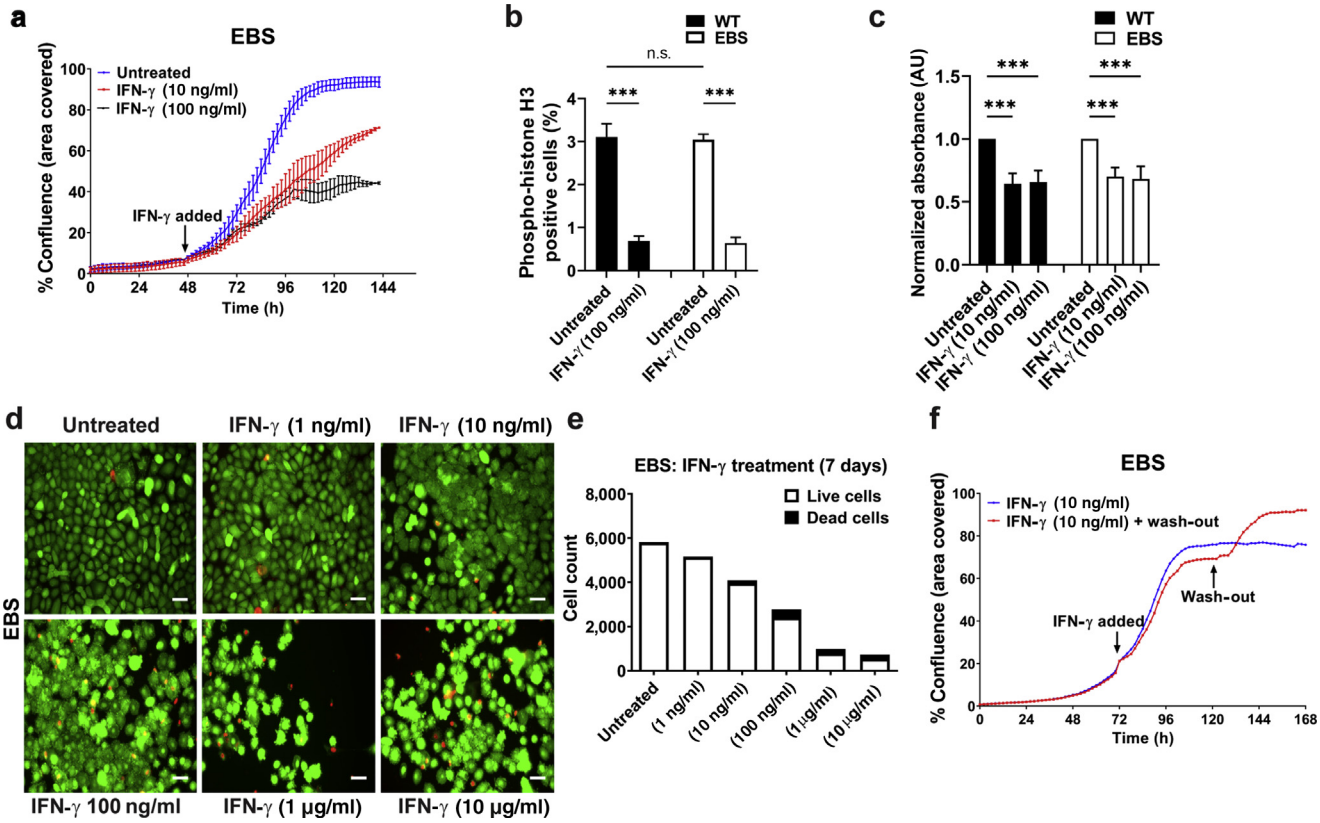

Figure 5. IFN-γ treatment reduces EBS cell proliferation and metabolic activity. (**a**) EBS KC growth curves of ±IFN-γ treatment (concentrations indicated) for 4 days. Mean ± SD, n = 2 per group. (**b, c**) Measurements of proliferative (phospho-histone H3 (Ser10)-positive) and viability/metabolism in WT and EBS KCs ± IFN-γ treatment (concentrations indicated) for 7 days. Normalized absorbance values (against untreated group) presented as AU. Mean ± SD, n = 3 per group in (**b**); n = 9 per group in (**c**). $^{***}P < 0.001$ versus untreated group (ANOVA). (**d**) LIVE/DEAD assay on EBS KCs ± IFN-γ treatment (concentrations indicated) for 7 days. Calcein (green, live) and ethidium homodimer-1 (red, dead) staining. Bar = 40 µm. (**e**) Cell count (live and dead cells)/group. (**f**) EBS KC growth curves after 96 h IFN-γ (10 ng/ml) treatment or with IFN-γ wash-out and fresh medium replacement at 48 h. AU, arbitrary unit; EBS, epidermolysis bullosa simplex; h, hour; n.s., nonsignificant; WT, wild type.

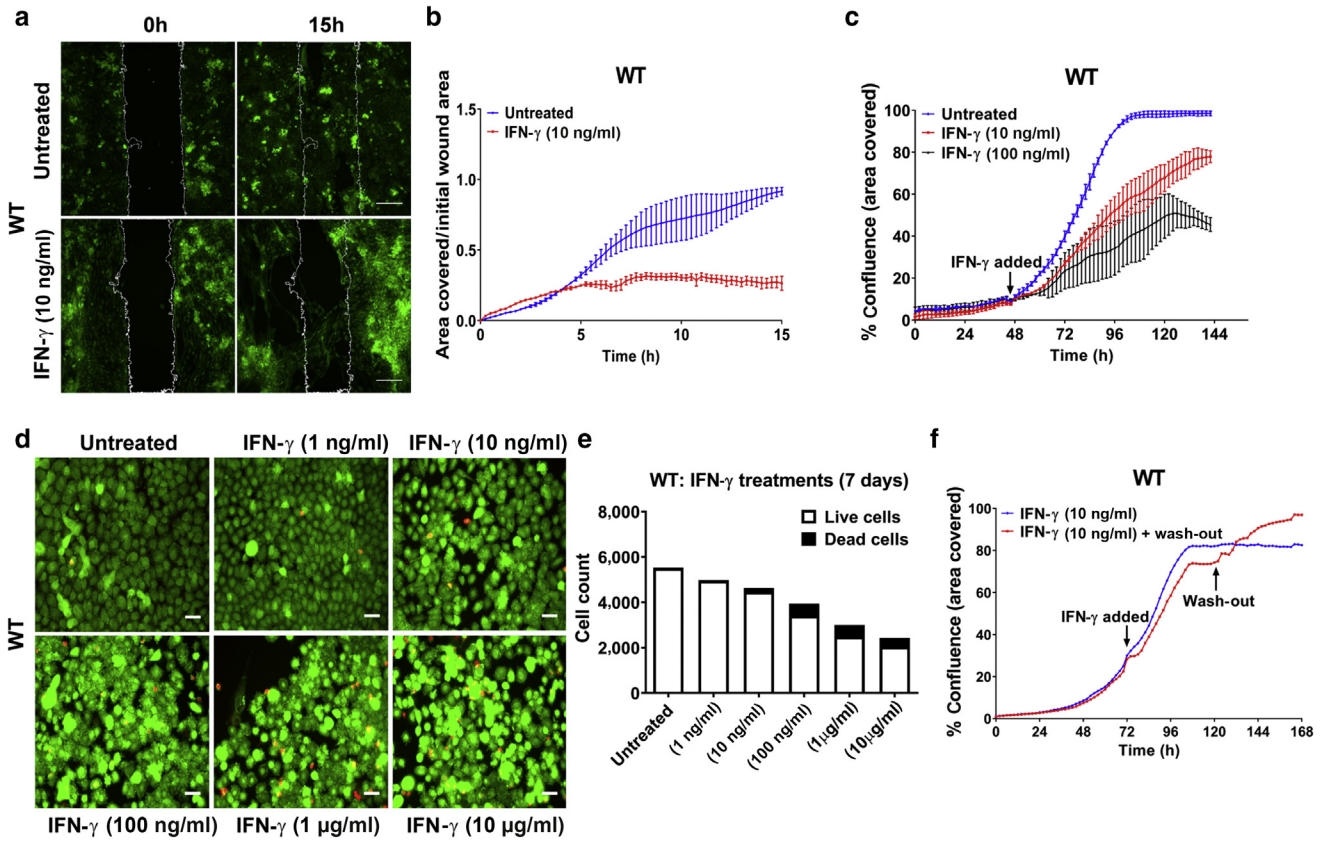

Figure 6. IFN-γ treatment reduces WT cell proliferation and delays wound closure. (**a, b**) Sequential images and graphs of WT KCs closing a wound gap, ± IFN-γ (10 ng/ml) added 48 h before closure was initiated on removal of the silicone culture insert. 0 h shows initial wound gap, whereas 5–15 h show remaining wound gap. Mean ± SD, n = 2 different fields from same wound gap. Bar = 200 μm. (**c**) WT KC growth curves of ± IFN-γ (concentrations indicated) for 4 days. Mean ± SD, n = 2 per group. (**d**) LIVE/DEAD assay on WT KCs ± IFN-γ (concentrations indicated) for 7 days. Calcein (green, live) and ethidium homodimer-1 (red, dead) staining. Bar = 40 μm. (**e**) Cell count (live and dead cells)/group. (**f**) WT KC growth curves after 96 h IFN-γ (10 ng/ml) treatment or with IFN-γ wash-out and fresh medium replacement at 48 h. h, hour; WT, wild type.

organotypics or controls without IFN-γ treatment (data not shown). These results suggest that IFN-γ constitutes a major cofactor that increases the fragility of sheets of EBS KCs in vitro.

IFN-γ reduces EBS cell proliferation and metabolic activity

As previously reported, IFN-γ, like other types of IFN, actively reduces cell proliferation as part of an immune antiviral response (Hattori et al., 2002; reviewed by Schroder et al., 2004). IncuCyte (Essen BioScience, Ann Arbor, MI) live imaging showed that cells treated with increasing doses of IFN-γ have lower overall cell coverage (% confluence) (Figures 5a and 6c), even though we observed a concurrent increase in the area covered by each cell (Figure 3a–c), that is, the total cell number is lower. Immunocytochemistry with an antibody to phospho-histone H3 (Ser10), a known marker of proliferation, showed a smaller population of mitotic cells (Figure 5b). This also correlated with reduced cell proliferation indicated by growth curves (Figure 5a), which was found to be reversible on wash-out of IFN-γ; removing IFN-γ after 48 hours of treatment restored proliferation of both EBS and WT KCs (Figure 5f and 6f). Results from cell viability/metabolism assays revealed that most of the IFN-γ–treated cells were less metabolically active than untreated cells (Figure 5c). LIVE/DEAD cell viability assays (Thermo Fisher Scientific, Waltham, MA) showed that IFN-γ treatment led to between ~3.5% (at 10 ng/ml) and ~13.5% (at 100 ng/ml) cell death (Figures 5d and e and 6d and e) in comparison to ~0.6% cell death in the untreated control cells. These findings suggest that as well as the less effective gap closure in these IFN-γ treated cells (Figures 3e and f and 6a and b), IFN-γ also slows down cell proliferation and metabolic activity.

Humanized IFN-γ blocking antibody attenuates IFN-γ–induced mutant keratin protein aggregation

Skurkovich and Skurkovich (2007) previously tested IFN-γ blocking antibodies for treatment of skin disorders, including dystrophic EB. We therefore investigated the effect of a neutralizing mouse mAb to human IFN-γ to improve the EBS phenotype in culture. A mAb to IFN-γ, known as F1, was generated earlier (Larina et al., 2015), and this was successfully humanized without loss of affinity (patent pending). A stable cell line producing the humanized antibody F1Hu2FA was developed from the CHO DG44 cell line using fluorescent clone selection with several subsequent rounds of dihydrofolate reductase/methotrexate gene amplification. Antibodies were isolated from the culture supernatant using Protein A affinity chromatography, yielding a homogeneous monomeric form of IgG1 (referred to henceforth as HuMab) (Figure 7a). The homogeneity of the F1Hu2FA antibody was

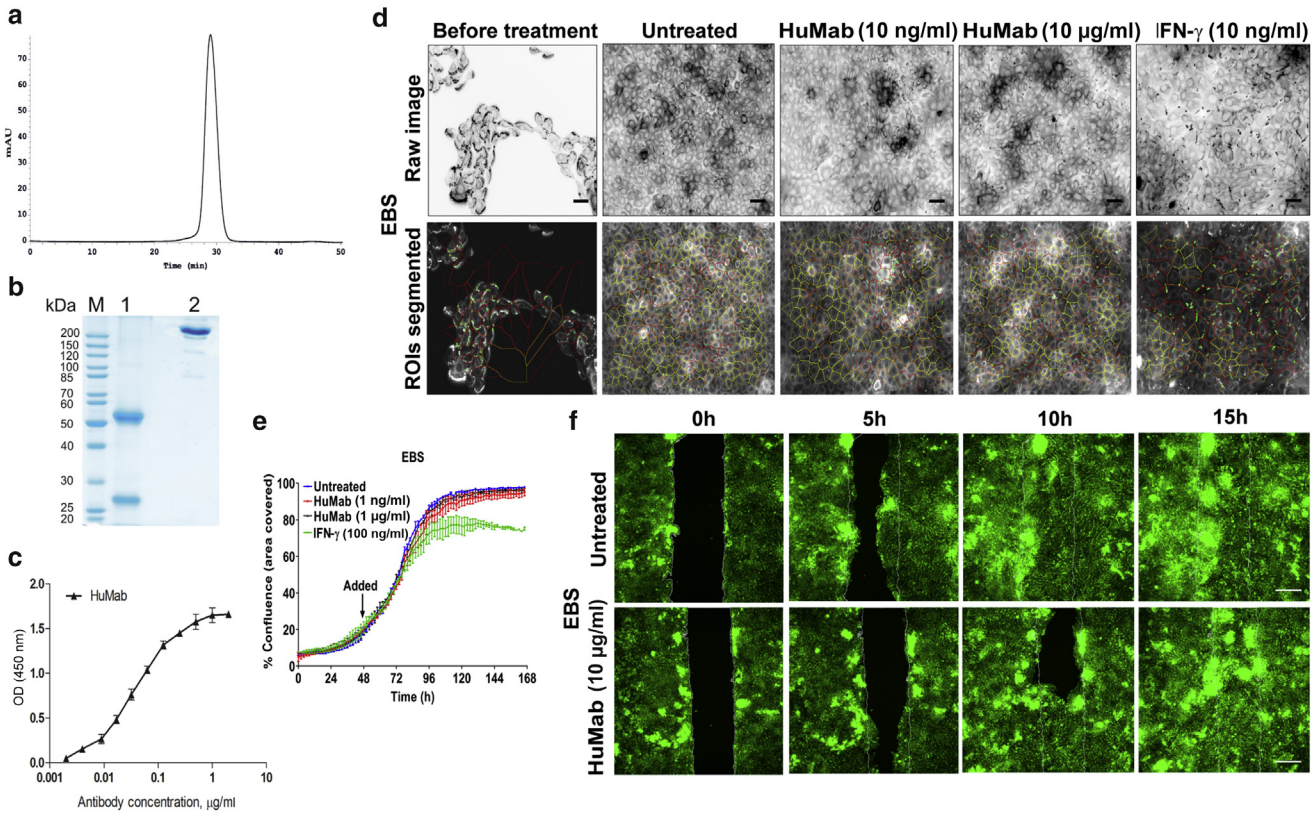

Figure 7. Purified humanized mAb to IFN-γ does not affect cell physiology and directional cell migration. (**a**) Analytical size-exclusion chromatography of affinity-purified antibody F1Hu2FA (HuMab) using Superdex 200-10/300 GL column. (**b**) SDS-PAGE (10%) of purified antibody: 1 indicates HuMab under reducing conditions (β-mercaptoethanol), 2 indicates HuMab under nonreducing conditions, and M indicates molecular weight marker. (**c**) Binding activity of HuMab for human IFN-γ (ELISA). The chromogenic reaction was generated by the horseradish peroxidase conjugated with the secondary antibody specific to the human kappa light chain of the humanized IgG, in the presence of 3,3′,5,5′-tetramethylbenzidine. (**d**) Subconfluent EBS KCs (before treatment) ± HuMab (10 µg/ml) or IFN-γ (10ng/ml) treatment for 7 days (inverse grayscale). Bar = 40 µm. Images segmented using CellProfiler scoring ROIs with (red) or without (yellow) aggregates. (**e**) EBS KC growth curves of ± IFN-γ (100 ng/ml) or with HuMab (concentrations indicated) over 120 h. Mean ± SD, n = 2 per group. (**f**) Sequential images of EBS KCs closing a wound gap, ± HuMab (10 µg/ml) added 48 h before closure was initiated on removal of the silicone culture insert. Zero h shows initial wound gap, whereas 5–15 h show remaining wound gap. Bar = 200 µm. EBS, epidermolysis bullosa simplex; h, hour; mAU, milli arbitrary unit; min, minute; OD, optical density; ROI, region-of-interest; WT, wild type.

confirmed using analytical gel filtration (Figure 7b). The ability of HuMab to bind human IFN-γ in vitro was confirmed by ELISA using increasing concentrations of HuMab (Figure 7c).

We tested the effects of HuMab treatment on KCs in tissue culture and showed that HuMab alone (up to 10 µg/ml) does not interfere with basic EBS or WT KC physiology as seen by the ability of cells to grow to full confluence and exhibit directional cell migration (Figure 7d–f). We therefore examined the ability of HuMab to neutralize the aggregate-inducing activity of IFN-γ. When added to the EBS disease model cells together with IFN-γ, HuMab protected the EBS cells from showing the increased mutant keratin aggregate formation that was seen on treatment with IFN-γ alone (Figure 8a). Different concentrations of HuMab were titrated for effectiveness over 7 days on EBS KCs in the presence of 10 ng/ml IFN-γ. We observed a dose–response relationship in the number of cells with keratin aggregates; at 1 µg/ml HuMab + 10 ng/ml IFN-γ, the detrimental effect of IFN-γ was greatly reduced (Figure 8b). A distinct decrease in phosphorylated STAT1 (Tyr701) levels was observed in IFN-γ–treated WT and EBS KCs when 5 µg/ml HuMab or 10 µg/ml HuMab was also present (Figure 8c and d). A similar downward trend was also observed in expression of stress response keratin 17 over 5 days in both cell lines (Figure 8c).

IFN-γ blocking antibody improves cell–cell adhesion, rescues cell growth, and accelerates wound closure in the presence of IFN-γ

HuMab was examined for its capacity to improve cell junctions in EBS KCs. Treatment with HuMab restored β-catenin and desmoplakin localization to the junctions of EBS KCs in the presence of IFN-γ, in parallel with a reduction of cells with keratin aggregates observed (Figure 9a and b). This relocalization of junction proteins to cell–cell adhesions could also be seen in WT KCs (Figure 10a and b). HuMab was also tested for its ability to neutralize the cell coverage reduction activity of IFN-γ. In both EBS and WT KCs, it was observed that cell coverage was restored almost to control levels when these cells were simultaneously incubated with both IFN-γ and HuMab (Figures 9c and 10c). Blocking IFN-γ with HuMab also increased wound closure rates in culture, and the speed of directional wound closure was restored to the level seen without IFN-γ (Figures 9d and e and 10d and e).

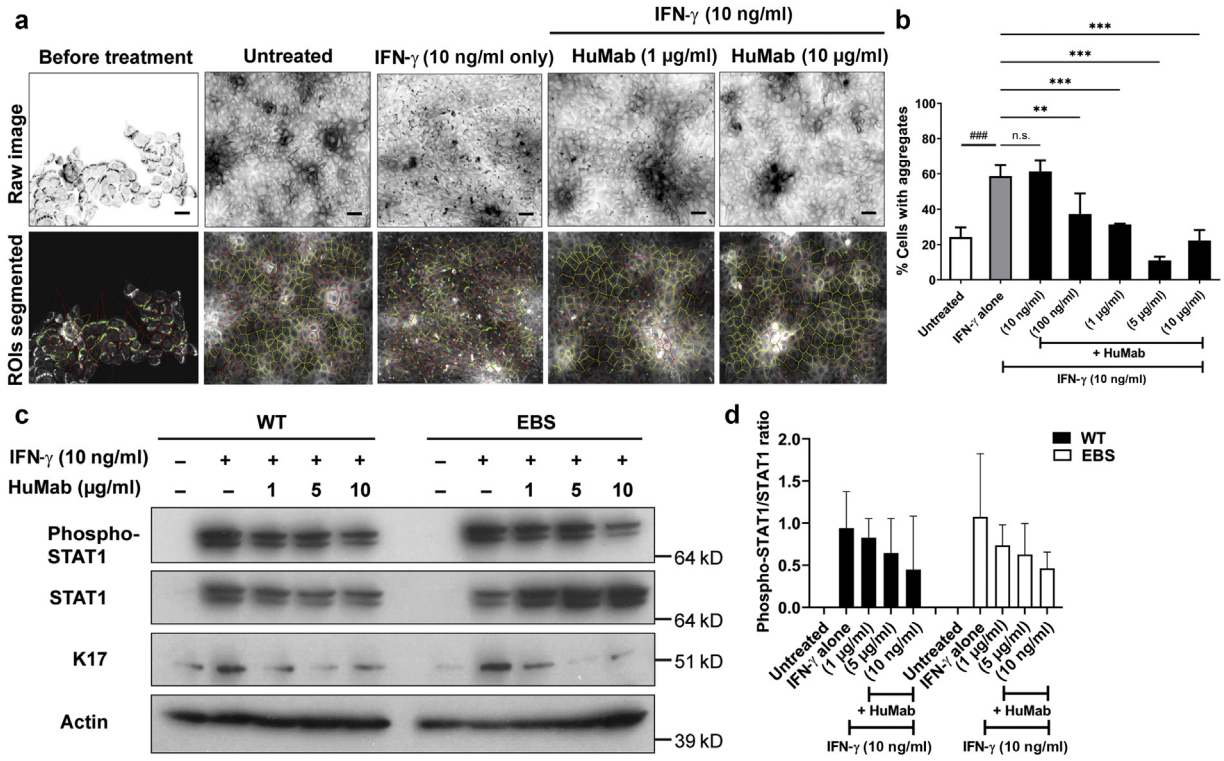

Figure 8. Humanized IFN-γ blocking antibody attenuates IFN-γ–induced mutant keratin protein aggregation and stress protein expression. (**a**) Subconfluent EBS KCs (before treatment) ± IFN-γ (10 ng/ml) treatment or treatment with IFN-γ + HuMab (concentrations indicated) for 7 days (inverse grayscale). Images segmented using CellProfiler scoring ROIs with (red) or without (yellow) aggregates. Bar = 40 μm. (**b**) At least 10,000 cells per group counted. Mean ± SD, n = 3 per group. $^{###}P < 0.001$ versus untreated group; $^{**}P < 0.01$ and $^{***}P < 0.001$ for IFN-γ + HuMab (concentrations indicated) versus IFN-γ alone group (ANOVA). (**c**) Immunoblotting phospho-Tyr701 STAT1, total STAT1, and K17 proteins in WT and EBS cell lysates ± IFN-γ (10 ng/ml) or with IFN-γ + HuMab (concentrations indicated) for 5 days. Actin as loading control. (**d**) Ratios of densitometry values (phospho-STAT1/STAT1) obtained using ImageJ. Mean ± SD, n = 2 per group. EBS, epidermolysis bullosa simplex; K17, keratin 17; n.s., non significant; ROI, region-of-interest; STAT, signal transducer and activator of transcription; WT, wild type.

Anti–IFN-γ potential for reducing blistering of EBS skin

KCs with EBS-associated mutations in *K14* or keratin 5 gene *K5* have been documented to show constitutive cell stress, with heightened responses to secondary applied experimental stress such as osmotic stress, heat shock, and scratch-wound disruption (D'Alessandro et al., 2002; Liovic et al., 2009; Morley et al., 2003). EBS KCs also show rapid remodeling of keratin-desmosome systems in response to mechanical stress (Russell et al., 2004). Although these features are thought to be initiated by a stress response induced by the misfolded mutant protein, the appearance of IFN-γ in serum and blister fluid of patients with EB (Annicchiarico et al., 2015; Esposito et al., 2016) suggest that EBS epidermis may secondarily be exposed to the elevated levels of IFN-γ, coming from immune cells stimulated by KC stress signaling. The findings described in this study provide evidence that elevated IFN-γ is likely to be detrimental to the course of the disease and may contribute to the observed mechanical fragility of the skin of patients with EBS by triggering changes associated with destabilization of cell–cell attachments. In patients with EBS, heightened levels of systemic IFN-γ may have significant effects on cellular cohesion and tissue integrity in patients with EBS in vivo, exacerbating the baseline stress differences arising from the EBS cells' constitutive processing of misfolding keratin protein owing to mutations. Thus, the inflammation-associated IFN-γ would increase the acantholysis observed in EBS epidermis and increase the epidermal instability, raising the risk of mechanical stress–induced epidermolysis and skin breakdown.

Therapies aimed at reducing inflammation in patients with EB are now emerging, for example, therapies based on IL-1β suppression with anti-inflammatory molecules, for the treatment of patients with EBS (Lettner et al., 2013; Wally et al., 2013a). Clinical trials currently suggest that anti-inflammatory molecules may be able to reduce the incidence of skin blistering of patients with EBS in vivo (Wally et al., 2013a). Treatment of patients with EBS generalized severe with apremilast (blocking cyclic adenosine monophosphate phosphodiesterase-4 and T-helper 1/T-helper 17 activation) was also reported to be effective (Castela et al., 2019). Although the correlation between IL-1β and EBS disease has been studied in vitro (Lettner et al., 2013; Wally et al., 2013b), little is known about the role and implications of IFN-γ in EBS.

A therapeutic approach that aims to block IFN-γ function may therefore be a viable strategy for reducing skin fragility. The anti–IFN-γ mAb described in this study is already humanized and thus represents a potentially valuable therapeutic agent that could be directly administered in patients with EBS, if an effective dose window can be identified that does not produce harmful side-effects. Such immunotherapy would be predicted to improve the skin condition of patients

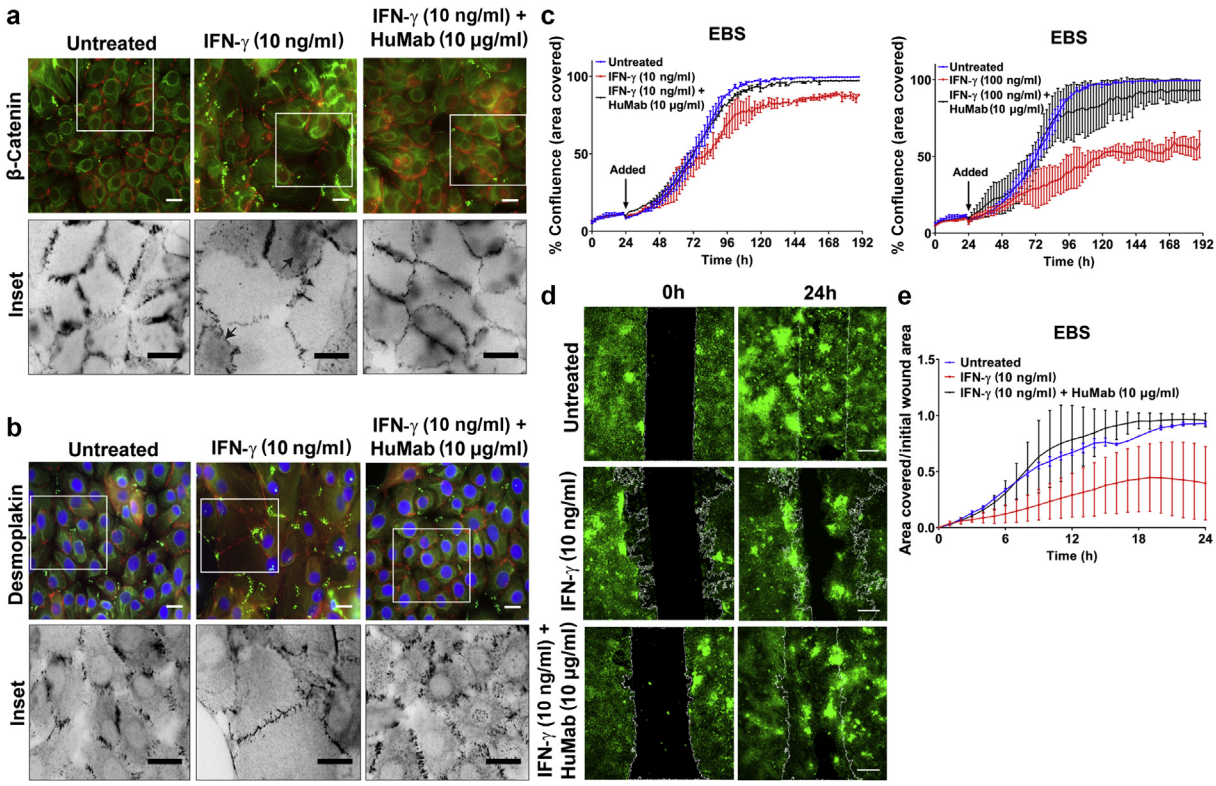

Figure 9. Humanized IFN-γ blocking antibody improves EBS cell–cell adhesion, rescues cell growth, and promotes efficient wound closure in the presence of IFN-γ. (**a, b**) EBS KCs ± IFN-γ (10 ng/ml) or with IFN-γ + HuMab (concentrations indicated) for 7 days show immunostaining of (**a**) β-catenin (some nuclear localization are indicated by black arrows) and (**b**) desmoplakin I/II. Inset shows inverse grayscale of ROIs. Bar = 20 μm. (**c**) EBS KC growth curves of ±IFN-γ or with IFN-γ + HuMab (concentrations indicated) over 148 h. Mean ± SD, n = 2 per group. (**d, e**) Sequential images and graphs of EBS KCs closing a wound gap, ± IFN-γ (10 ng/ml) or with IFN-γ + HuMab (concentrations indicated) added 48 h before closure was initiated on removal of the silicone culture insert. 0 h denotes initial wound gap, whereas 6–24 h show remaining wound gap. Bar = 200 μm. Mean ± SD, n = 2 different fields within same wound gap. EBS, epidermolysis bullosa simplex; h, hour; ROI, region-of-interest.

with EBS by limiting skin blistering, alleviating pain associated with blisters, and promoting the healing of existing blisters. Use of this mAb may also be efficacious for other inflammatory skin diseases because our findings suggest it would be worthwhile investigating HuMab applications for inflammation in a wider context.

MATERIALS AND METHODS

Cells and culture

N/TERT-1 cells (gifted by JG Rheinwald, Harvard Medical School, Boston, MA) (Dickson et al., 2000) were engineered to stably express GFP-coupled WT (GFP-K14 WT) and mutant (GFP-K14 R125P) K14 as described elsewhere (Tan, 2012; Tan et al., 2016); in this study, these are referred to as WT KCs and EBS KCs, respectively. Cells were cultured at 37 °C in 5% carbon dioxide without fibroblast feeder cells, using keratinocyte serum-free medium (KSFM; (Life Technologies, Carlsbad, CA) supplemented with 25 μg/ml of bovine pituitary extract, 0.2 ng/ml of human recombinant EGF, 0.4 mM of calcium chloride, and 1% penicillin/streptomycin (Life Technologies) (Dickson et al., 2000). Cell lines were regularly checked for mycoplasma infection whenever new vials were thawed and cultured, using the MycoAlert PLUS Mycoplasma Detection Kit (Lonza Bioscience, Basel, Switzerland).

IFN-γ monoclonal antibody production and purification

For humanized monoclonal antibody production, CHO DG44 cells stably producing recombinant humanized antibody F1Hu2FA (HuMab) were cultivated in serum-free CD OptiCHO medium (Thermo Fisher Scientific) supplemented with 6 mM GlutaMax (Gibco, Waltham, MA) and 0.1% pluronic F-68 (Gibco) in spinner flasks for 14 days. Recombinant F1Hu2FA antibody was purified from culture medium using protein A affinity capture on HiTrap rProtein A FF (GE Healthcare, Chicago, IL) 5 ml column. To verify homogeneity of affinity-purified antibodies, we performed analytical size-exclusion chromatography using Superdex 200-10/300 GL (GE Healthcare) column. Purified HuMab antibody was buffer-exchanged in PBS. Finally, the HuMab samples were sterilized through 0.22 μm surfactant-free cellulose acetate membrane (Corning, New York, NY). Sample concentration measurements were performed using NanoDrop 2000 (Thermo Fisher Scientific).

Other antibodies

Other antibodies used were as follows: mouse mAbs used were anti-K14 (Purkis et al., 1990), anti-desmoplakin (11-5F) (gifted by David Garrod, The University of Manchester, Manchester, United Kingdom), anti–β-actin (clone AC-15, number A5441, Sigma-Aldrich, St. Louis, MO), anti–β-catenin (number ab16051, Abcam, Cambridge, United Kingdom; clone 14, number 610153, BD Biosciences, San Jose, CA), and anti–keratin 17 (number NCL-L-CK17, Leica Biosystems, Richmond, IL); rabbit mAbs or polyclonal antibodies used were anti–phospho-STAT1 (Tyr701) (clone D4A7, number 7649, Cell Signaling Technology, Danvers, MA), anti-STAT1 (clone D1K9Y, number 14994, Cell Signaling Technology), and anti-

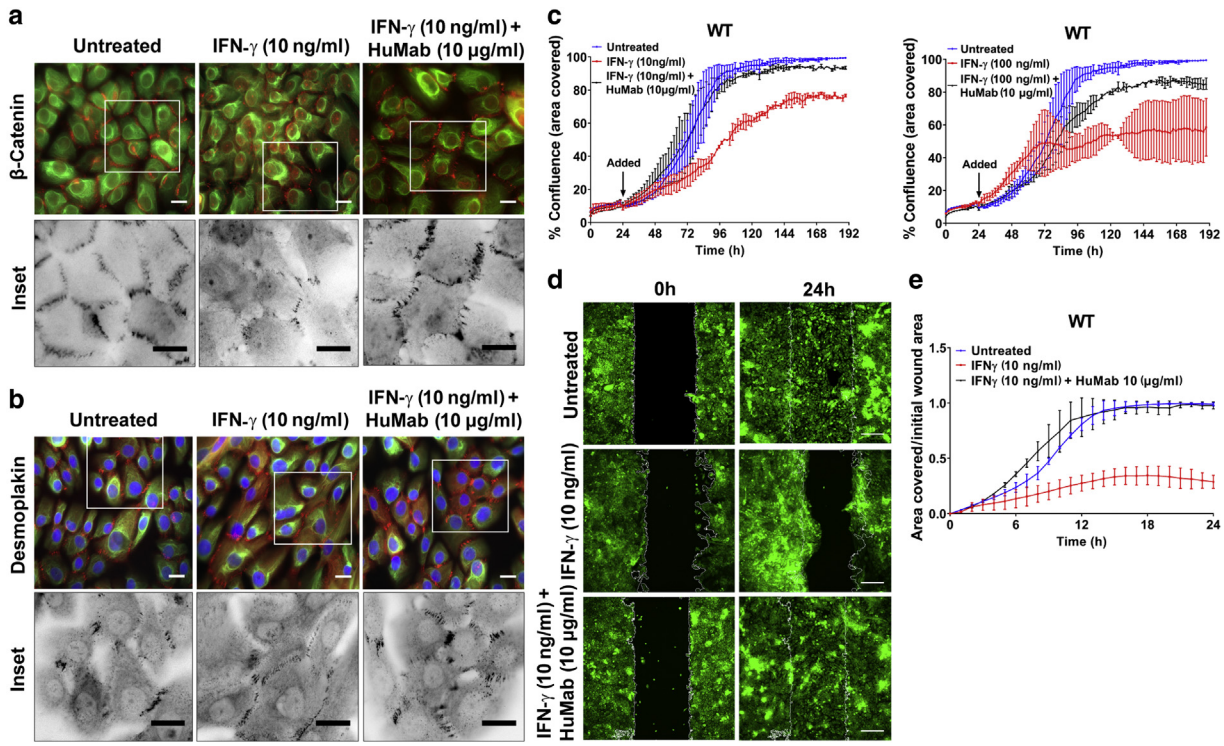

Figure 10. IFN-γ blocking antibody increases WT cell–cell adhesion, rescues cell growth, and promotes efficient wound closure in the presence of IFN-γ. (**a, b**) WT KCs ± IFN-γ (10 ng/ml) treatment or treatment with IFN-γ + HuMab (concentrations indicated) for 7 days show immunostaining of (**a**) β-catenin and (**b**) desmoplakin I/II. Inset shows inverse grayscale of ROIs. Bar = 20 μm. (**c**) WT KC growth curves of ± IFN-γ treatment or treatment with IFN-γ + HuMab (concentrations indicated) over 148 h. Mean ± SD, n = 2 per group. (**d, e**) Sequential images and graphs of WT KCs closing a wound gap, ± IFN-γ (10 ng/ml) or with IFN-γ + HuMab (concentrations indicated) added 48 h before closure was initiated on removal of the silicone culture insert. 0 h denotes initial wound gap, whereas 6–24 h show remaining wound gap. Bar = 200 μm. (**e**) Mean ± SD, n = 2 different fields within same wound gap. h, hour; ROI, region-of-interest; WT, wild type.

phospho-Histone H3 (Ser10) Antibody (clone MC463, number 04-817, Merck Millipore, Burlington, MA); secondary antibodies used were goat anti-rabbit IgG (H+L) Alexa Fluor 594 (number A-11037, Thermo Fisher Scientific); goat anti-mouse IgG (H+L) Alexa Fluor 568 (number A-11031, Thermo Fisher Scientific); Anti-Mouse IgG (H+L), HRP Conjugate (number W4021, Promega, Madison, WI); and Anti-Rabbit IgG (H+L), HRP Conjugate (number W4011, Promega); and antibody to human kappa light chain conjugated to horseradish peroxidase was used in ELISA (kindly provided by Prof PG Sveshnikov, Russian Research Center for Molecular Diagnostics and Treatment, Moscow, Russia).

Indirect ELISA

Microtiter 96-well Maxisorp plates (Thermo Fisher Scientific) were coated with 100 μl of 2.5 μg/ml recombinant human IFN-γ (PeproTech, London, United Kingdom) in 100 mM bicarbonate buffer at pH 9.6 and temperature 4 ℃ overnight. After blocking plates with 3% BSA in PBS for 1 hour at room temperature, HuMab antibody samples diluted in blocking buffer were added to each well and incubated at room temperature for 1 hour with shaking. After washing, 100 μl of goat anti-human IgG (whole molecule)-peroxidase conjugate (1:10,000 [v/v]; Sigma-Aldrich) were added to each well and incubated at room temperature for 1 hour. Finally, 100 μl of 3,3′,5,5′-tetramethylbenzidine substrate (Immunotech, Moscow, Russia) were added to each well and incubated for 10 minutes. The reaction was stopped by the addition of 50 μl of 10% sulfuric acid. The optical density was measured at 450 nm in an ELISA plate reader (Microplate reader 680, Bio-Rad Laboratories, Hercules, CA).

Immunoblotting

WT or EBS cells seeded on 60-mm dish were washed in ice-cold PBS, scraped, and collected in 1 ml of PBS. The cell suspensions were then centrifuged at 9,000 r.p.m. for 5 minutes. The cell pellets were resuspended in 100 μl of lysis buffer containing 20 mM Tris-hydrochloride (pH 7.6), 140 mM sodium chloride, 5 mM EDTA, 1% (v/v) NP-40, and 0.5% (w/v) sodium deoxycholate supplemented with cOmplete and Mini (EDTA-free) protease and phosphatase inhibitor cocktail tablet (Thermo Fisher Scientific) per 10 ml lysis buffer. The cells were then lysed on ice for 15 minutes before being separated by centrifugation at 16,000*g* for 15 minutes at 4 °C. The supernatants were then homogenized through a QIAshredder column tube (QIAGEN, Hilden, Germany) by centrifugation at 9,000 r.p.m. for 5 minutes at 4 °C. Protein concentration of the supernatants was then determined by BCA assay (Thermo Fisher Scientific) and standardized using BSA. SDS-PAGE and immunoblotting were performed as previously described (Tan et al., 2021). Protein levels were quantified from images of immunoblots using ImageJ software (National Institutes of Health, Bethesda, MD) (Schneider et al., 2012). Primary antibodies (sources aforementioned) were used at the following dilutions: anti-K14 (LL001) (1:250), anti–phospho-STAT1 (1:1,000), anti-STAT1 (1:1,000), anti–β-actin (1:5,000), anti-K17 (1:20), anti-desmoplakin (1:1,000), and anti-β-catenin (1:1,000). Secondary antibodies were used at the following

dilutions: Anti-Mouse IgG (H+L), HRP Conjugate (1:1,000) and Anti-Rabbit IgG (H+L), HRP Conjugate (1:1,000).

Immunostaining

WT or EBS cells seeded on glass coverslips were fixed with either 4% paraformaldehyde (Sigma-Aldrich) in PBS for 10 minutes at room temperature, permeabilized with 0.1% Triton X-100 for 10 minutes, or fixed with ice-cold methanol in 4 ℃ for 10 minutes. Cells were blocked in blocking buffer (3% goat serum in PBS) before incubation with primary antibodies overnight. Primary antibodies were used at the following dilutions: anti-K14 (LL001) (no dilution), anti-desmoplakin I/II (11-5F) (1:100), anti−β-catenin (1:50), and Anti-phospho-Histone H3 (Ser-10) Antibody (1:500). Cells were then incubated with either goat anti-mouse IgG (H+L) Alexa Fluor 568 (1:500) or goat anti-rabbit IgG (H+L) Alexa Fluor 594 (1:500) antibodies in the dark, followed by DAPI staining, with PBS washes in between. All coverslips were mounted on glass-slides with hydromount (Electron Microscopy Sciences, Hatfield, PA), with 2.5% DABCO (1,4-diazabicyclo[2.2.2]octane) (Sigma Aldrich, St. Louis, MO). Images were acquired on an inverted DeltaVision epifluorescence microscope, attached to a Photometrics CCD camera (CoolSNAP HQ2) with a SEDAT filter set, or AxioImager ZI (Carl Zeiss, Oberkochen, Germany) with Axio Cam 506 mono or an inverted Axiovert 200M microscope (Carl Zeiss) that is equipped with a Zeiss motorized Z-stage and postanalyzed using ImageJ software.

IFN-γ treatments

For subconfluent studies, 5×10^4 of either WT or EBS cells were seeded on each well of a 24-well plate (Thermo Fisher Scientific). After 72 hours, the cells were treated with human recombinant IFN-γ (Life Technologies) at concentrations 10 ng/ml to 100 ng/ml and monitored over 7 days.

For postconfluent studies, 5×10^4 EBS cells were seeded on each well of a 24-well plate). Cells were cultured for 2 days after confluence until most keratin aggregates disappeared. Human recombinant IFN-γ was added to triplicate wells at concentrations 10 ng/ml to 100 ng/ml and monitored over 3 days.

The cells were fixed in 4% paraformaldehyde for 10 minutes and stained with Image-IT LIVE Plasma Membrane and Nuclear Labelling Kit following the manufacturer's protocol (Thermo Fisher Scientific).

High content imaging and semiautomated analysis

Fluorescent images of EBS cells with keratin aggregates were acquired using the Olympus IX-81 high content screening inverted microscope (Olympus, Tokyo, Japan), attached with a Marzhauser Scan IM (120 × 100) motorized XY stage controlled by Ludl Mac5000 and a Photometrics CCD camera (CoolSNAP HQ2) with DAPI, EGFP, and TRITC filters. Fluorescent images were analyzed with customized algorithms written with ImageJ software for quantitative analysis of keratin aggregates in mutant cells (Tan et al., 2021). Alternatively, these images were analyzed using CellProfiler free open-source software (cellprofiler.org) to count keratin aggregates in mutant cells. Briefly, a custom pipeline was designed and applied to the images to identify three key features of a cell: the nucleus, plasma membrane, and keratin aggregates. These features are needed to determine the overall cell density (nuclear count), cell boundary (plasma membrane), and the number of keratin aggregates (GFP-tagged K14 protein) present in each cell identified within the cytoplasm. The CellProfiler software calculates the average number of keratin aggregates per cell and the percentage of cells containing keratin aggregates for each set of fluorescent images.

Cell proliferation and viability assays

For cell coverage assays, 5×10^4 per well of WT or EBS cells were seeded in 6-well plates (Thermo Fisher Scientific) and cultured at 37 °C and 5% carbon dioxide in IncuCyte. Cell coverage (%confluence) was monitored every 2 hours by taking phase-contrast images at ×10 magnification. After 72 hours, human recombinant IFN-γ was added at concentrations from 10 ng/ml to 100 ng/ml, and cells were cultured for 8 days. Wash-out experiments were conducted on two wells from each cell line at 48 hours after adding IFN-γ: media from one IFN-γ−treated well was replaced with fresh medium without IFN-γ, and fresh medium with IFN-γ was added to the second well of each cell line. The cells were further incubated in IncuCyte to continue tracking cell coverage.

Proliferation was directly measured by phospho-histone H3 (Ser10) levels. Images of WT or EBS cells immunostained with rabbit phospho-histone H3 (Ser10) antibody were acquired on an inverted DeltaVision epifluorescence microscope and analyzed using ImageJ software and Prism 9.0 (GraphPad Software, San Diego, CA).

For cell viability assays, 3×10^3 of either WT or EBS cells were seeded in each well of a 96-well plate (Thermo Fisher Scientific). After 72 hours, 10 ng/ml or 100 ng/ml of human recombinant IFN-γ was added to the wells, and the cells were incubated for another 7 days. After 7 days, cell viability/metabolism assay was performed using Celltiter 96 AQueous One Solution Cell Proliferation Assay (Promega) according to the manufacturer's instructions. Briefly, 20 μl of Celltiter 96 AQueous One Solution Reagent was added to each well and incubated for 90 minutes. The absorbance was then recorded in a 96-well plate reader at 490 nm, and statistical results were analyzed using Prism 9.0.

For LIVE/DEAD assays, 5×10^3 of either WT or EBS cells were seeded on each well of a 24-well plate. After 72 hours of seeding, cells were treated with human recombinant IFN-γ at concentrations ranging from 1 ng/ml to 10 μg/ml for 7 days. After 7 days, cells were subjected to LIVE/DEAD cytotoxicity kit according to the manufacturer's instructions. Briefly, the wells were washed once with PBS, before a solution containing 2 μM calcein AM, 1 μM ethidium homodimer-1, and 1 μM Hoechst 33342 (Thermo Fisher Scientific) in PBS was added to each well and cells were incubated for 45 minutes in the dark at room temperature. Fluorescent images in each well were then acquired using the Olympus IX-81 high content screening inverted microscope, and postanalyzed using ImageJ software as previously described (Tan et al., 2021).

Wound healing assay (barrier removal)

Wound closure assay was done using a removable 2-chamber silicone insert with a defined 500 μm cell-free gap, which was manually placed within each well of a 24-well plate. WT or EBS cells were seeded onto the culture insert (ibidi) in 100 μl of KSFM per chamber, and the outsides of the insert filled with cells. After 72 hours, the KSFM medium was aspirated gently from the chambers and switched to DF-K experimental medium (1:1 v/v of KSFM and DF-K medium, which consist of equal volumes of DMEM and Ham's F12 medium containing 0.2 ng/ml of EGF, 1% L-glutamine, 25 μg/ml of bovine pituitary extract, and 0.4 mM of calcium chloride) (Dickson et al., 2000), containing either 10 ng/ml human recombinant IFN-γ or 10 ng/ml human recombinant IFN-γ + HuMab (10 μg/ml). After 48 hours incubation, the silicone insert was removed using sterilized

tweezers. The dishes were then imaged on an Olympus IX-83 live-cell imaging inverted microscope (Olympus) in an enclosed chamber at 37 °C and 5% carbon dioxide. Fluorescent and phase-contrast images were acquired at ×10 magnification and postanalyzed using ImageJ software macro that derived the initial wound area between two migrating fronts of the in vitro wound and the area of wound region covered over time and presented as ratio of area covered-to-initial wound area.

Dispase-based dissociation assay

Of either WT or EBS cells, 2×10^5 was seeded in 35-mm dishes and grown to 100% confluence in KSFM medium before switching to DF-K experimental medium (1:1 v/v of KSFM and DF-K medium, which consist of equal volumes of DMEM and Ham's F12 medium containing 0.2 ng/ml of EGF, 1% L-glutamine, 25 μg/ml of BPE, and 0.4 mM of calcium chloride) (Dickson et al., 2000) containing either 100 ng/ml human recombinant IFN-γ) or left untreated and incubated for another 72 hours. After 72 hours incubation, the monolayers were washed with PBS and incubated in 2.4 U/ml Dispase II (neutral protease, grade II) (F. Hoffmann-La Roche, Basel, Switzerland) for 30 minutes at 37 °C. The detached monolayers were carefully washed with PBS and transferred to 15 ml conical tubes filled with 5 ml PBS. The tubes were attached to a rocker and subjected to 50 inversion cycles. The fragments were then imaged using a Chemidoc MP Imager with a green fluorescent filter (Bio-Rad Laboratories). The number of fragments was quantitated on the basis of a minimum size requirement using a batch processing macro written with ImageJ as previously described (Tan et al., 2021).

Statistical analyses

Data analysis was performed by either unpaired Student's *t*-test for two groups or one-way ANOVA, followed by post hoc Tukey's test for multiple comparisons of at least three groups using Prism 9.0. $P < 0.05$ was considered statistically significant.

Data availability statement

No datasets were generated or analyzed during this study.

ORCIDs

Cedric Badowski: http://orcid.org/0000-0002-5250-2104
Tong San Tan: http://orcid.org/0000-0003-2428-2308
Teimur Aliev: http://orcid.org/0000-0002-1753-9614
David Trudil: http://orcid.org/0000-0002-4114-8138
Maria Larina: http://orcid.org/0000-0002-5305-0293
Victoria Argentova: http://orcid.org/0000-0001-9969-4708
Muhammad Jasrie Firdaus: http://orcid.org/0000-0003-4843-9605
Paula Benny: http://orcid.org/0000-0001-9118-915X
Vivien S.T. Woo: http://orcid.org/0000-0001-8330-519X
E. Birgitte Lane: http://orcid.org/0000-0003-1457-2934

AUTHOR CONTRIBUTIONS

Conceptualization: CB, TST, DT, TA, EBL; Formal Analysis: CB, TST, TA, ML, VA, MJF, VSTW; Funding Acquisition: EBL; Investigation: CB, TST, ML, VA, MJF, VSTW, PB, TA, DT, EBL; Methodology: CB, TST, PB, DT, TA, ML, VA; Project Administration: CB, TST, DT, TA, EBL; Resources: DT, TA, ML, VA, EBL; Supervision: CB, TST, DT, TA, EBL; Validation: TST, MJF, ML, VA; Visualization: CB, TST, DT, TA, ML, VA, EBL; Writing - Original Draft Preparation: CB, DT, TA, EBL; Writing - Review and Editing: CB, TST, TA, DT, ML, VA, MJF, VSTW, PB, EBL

CONFLICT OF INTEREST

The authors state no conflict of interest.

ACKNOWLEDGMENTS

The authors thank Simon Denil for the statistical analyses and Paul MacAry for helpful discussions. The authors also thank John Lim and Graham Wright from the Agency for Science, Technology and Research (A*STAR; Singapore, Singapore) Microscopy Platform for advice on image segmentation algorithms, including macros written with Fiji software (ImageJ) for automated counting of keratin aggregates or cell fragments and quantification of in vitro wound area. The N/TERT-1 derived cell lines GFP-K14 WT and GFP-K14 R125P were initially described in Tan's doctoral thesis (Tan, 2012); images in Figure 1b also appeared in Woo's doctoral thesis (Woo, 2016). This work was supported by core funding from the Biomedical Research Council, Singapore to the former Institute of Medical Biology and the Skin Research Institute of Singapore (SRIS), Agency for Science, Technology and Research (A*STAR). Funding sources were not involved in the conduct of the research or writing of the manuscript. No payment was received from any pharmaceutical company or other for-profit agency to write this manuscript. This paper is dedicated to the memory of Simon Skurkovich (1922-2017).

SUPPLEMENTARY MATERIAL

Supplementary material is linked to the online version of the paper at www.jidonline.org, and at https://doi.org/10.1016/j.xjidi.2022.100096.

REFERENCES

Annicchiarico G, Morgese MG, Esposito S, Lopalco G, Lattarulo M, Tampoia M, et al. Proinflammatory cytokines and antiskin autoantibodies in patients with inherited epidermolysis bullosa. Medicine (Baltimore) 2015;94:e1528.

Anton-Lamprecht I, Schnyder UW. Epidermolysis bullosa herpetiformis Dowling-Meara. Report of a case and pathomorphogenesis. Dermatologica 1982;164:221–35.

Bonifas JM, Rothman AL, Epstein EH Jr. Epidermolysis bullosa simplex: evidence in two families for keratin gene abnormalities. Science 1991;254:1202–5.

Bonnekoh B, Huerkamp C, Wevers A, Geisel J, Sebök B, Bange FC, et al. Up-regulation of keratin 17 expression in human HaCaT keratinocytes by interferon-gamma. J Invest Dermatol 1995;104:58–61.

Castela E, Tulic MK, Rozières A, Bourrat E, Nicolas JF, Kanitakis J, et al. Epidermolysis bullosa simplex generalized severe induces a T helper 17 response and is improved by apremilast treatment. Br J Dermatol 2019;180:357–64.

Castro F, Cardoso AP, Gonçalves RM, Serre K, Oliveira MJ. Interferon-gamma at the crossroads of tumor immune surveillance or evasion. Front Immunol 2018;9:847.

Coulombe PA, Hutton ME, Letai A, Hebert A, Paller AS, Fuchs E. Point mutations in human keratin 14 genes of epidermolysis bullosa simplex patients: genetic and functional analyses. Cell 1991;66:1301–11.

D'Alessandro M, Russell D, Morley SM, Davies AM, Lane EB. Keratin mutations of epidermolysis bullosa simplex alter the kinetics of stress response to osmotic shock. J Cell Sci 2002;115:4341–51.

Dickson MA, Hahn WC, Ino Y, Ronfard V, Wu JY, Weinberg RA, et al. Human keratinocytes that express hTERT and also bypass a p16(INK4a)-enforced mechanism that limits life span become immortal yet retain normal growth and differentiation characteristics. Mol Cell Biol 2000;20:1436–47.

Eming SA, Krieg T, Davidson JM. Inflammation in wound repair: molecular and cellular mechanisms. J Invest Dermatol 2007;127:514–25.

Esposito S, Guez S, Orenti A, Tadini G, Scuvera G, Corti L, et al. Autoimmunity and cytokine imbalance in inherited epidermolysis bullosa. Int J Mol Sci 2016;17:1625.

Freedberg IM, Tomic-Canic M, Komine M, Blumenberg M. Keratins and the keratinocyte activation cycle. J Invest Dermatol 2001;116:633–40.

Hattori N, Komine M, Yano S, Kaneko T, Hanakawa Y, Hashimoto K, et al. Interferon-gamma, a strong suppressor of cell proliferation, induces upregulation of keratin K6, one of the inflammatory- and proliferation-associated keratins. J Invest Dermatol 2002;119:403–10.

Ishida-Yamamoto A, McGrath JA, Chapman SJ, Leigh IM, Lane EB, Eady RA. Epidermolysis bullosa simplex (Dowling-Meara type) is a genetic disease characterized by an abnormal keratin-filament network involving keratins K5 and K14. J Invest Dermatol 1991;97:959–68.

Kawakami Y, Oyama N, Ohtsuka M, Nakamura K, Kaneko F. Increased serum levels of interleukin-6, immunoglobulin and acute phase protein in patients with the severe clinical form of inherited epidermolysis bullosa. J Dermatol 2005;32:503–5.

Kirfel G, Herzog V. Migration of epidermal keratinocytes: mechanisms, regulation, and biological significance. Protoplasma 2004;223:67–78.

Lane EB. Keratin diseases. Curr Opin Genet Dev 1994;4:412–8.

Lane EB, Rugg EL, Navsaria H, Leigh IM, Heagerty AH, Ishida-Yamamoto A, et al. A mutation in the conserved helix termination peptide of keratin 5 in hereditary skin blistering. Nature 1992;356:244–6.

Larina MV, Aliev TK, Solopova ON, Pozdnyakova LP, Korobova SV, Yakimov SA, et al. **Нейтрализующие моноклональные и чимерные антитела к интерферону-γ человека** [Neutralizing monoclonal and chimeric antibodies to human interferon-γ]. Bioorg Khim [in Russian] 2015;41:316–26.

Letai A, Coulombe PA, McCormick MB, Yu QC, Hutton E, Fuchs E. Disease severity correlates with position of keratin point mutations in patients with epidermolysis bullosa simplex. Proc Natl Acad Sci USA 1993;90:3197–201.

Lettner T, Lang R, Klausegger A, Hainzl S, Bauer JW, Wally V. MMP-9 and CXCL8/IL-8 are potential therapeutic targets in epidermolysis bullosa simplex. PLoS One 2013;8:e70123.

Liovic M, D'Alessandro M, Tomic-Canic M, Bolshakov VN, Coats SE, Lane EB. Severe keratin 5 and 14 mutations induce down-regulation of junction proteins in keratinocytes. Exp Cell Res 2009;315:2995–3003.

Morley SM, D'Alessandro M, Sexton C, Rugg EL, Navsaria H, Shemanko CS, et al. Generation and characterization of epidermolysis bullosa simplex cell lines: scratch assays show faster migration with disruptive keratin mutations. Br J Dermatol 2003;149:46–58.

Platanias LC. Mechanisms of type-I- and type-II-interferon-mediated signalling. Nat Rev Immunol 2005;5:375–86.

Porter RM, Lane EB. Phenotypes, genotypes and their contribution to understanding keratin function. Trends Genet 2003;19:278–85.

Purkis PE, Steel JB, Mackenzie IC, Nathrath WBJ, Leigh IM, Lane EB. Antibody markers of basal cells in complex epithelia. J Cell Sci 1990;97:39–50.

Russell D, Andrews PD, James J, Lane EB. Mechanical stress induces profound remodelling of keratin filaments and cell junctions in epidermolysis bullosa simplex keratinocytes. J Cell Sci 2004;117:5233–43.

Schneider CA, Rasband WS, Eliceiri KW. NIH Image to ImageJ: 25 years of image analysis. Nat Methods 2012;9:671–5.

Schroder K, Hertzog PJ, Ravasi T, Hume DA. Interferon-gamma: an overview of signals, mechanisms and functions. J Leukoc Biol 2004;75:163–89.

Singer AJ, Clark RA. Cutaneous wound healing. N Engl J Med 1999;341:738–46.

Skurkovich B, Skurkovich S. Autoimmune diseases are connected with disturbances in cytokine synthesis, and therapy with IFN-gamma blockers is their main pathogenetic treatment. Ann N Y Acad Sci 2007;1109:167–77.

Tan TS. *Keratin remodelling in stress* [PhD thesis]. Singapore, Singapore: National University of Singapore; 2012.

Tan TS, Common JEA, Lim JSY, Badowski C, Firdaus MJ, Leonardi SS, et al. A cell-based drug discovery assay identifies inhibition of cell stress responses as a new approach to treatment of epidermolysis bullosa simplex. J Cell Sci 2021;134:jcs258409.

Tan TS, Ng YZ, Badowski C, Dang T, Common JE, Lacina L, et al. Assays to study consequences of cytoplasmic intermediate filament mutations: the case of epidermal keratins. Methods Enzymol 2016;568:219–53.

Wally V, Kitzmueller S, Lagler F, Moder A, Hitzl W, Wolkersdorfer M, et al. Topical diacerein for epidermolysis bullosa: a randomized controlled pilot study. Orphanet J Rare Dis 2013a;8:69.

Wally V, Lettner T, Peking P, Peckl-Schmid D, Murauer EM, Hainzl S, et al. The pathogenetic role of IL-1β in severe epidermolysis bullosa simplex. J Invest Dermatol 2013b;133:1901–3.

Werner NS, Windoffer R, Strnad P, Grund C, Leube RE, Magin TM. Epidermolysis bullosa simplex-type mutations alter the dynamics of the keratin cytoskeleton and reveal a contribution of actin to the transport of keratin subunits. Mol Biol Cell 2004;15:990–1002.

Woo ST. *Keratin 14 phosphorylation during mitosis and stress* [PhD thesis]. Singapore, Singapore: National University of Singapore; 2016.